Progress in Nuclear Energy xxx (2009) 1–13

Contents lists available at ScienceDirect

Progress in Nuclear Energy

journal homepage: www.elsevier.com/locate/pnucene

Three-dimensional *h*-adaptivity for the multigroup neutron diffusion equations

Yaqi Wang [a], Wolfgang Bangerth [b,*], Jean Ragusa [a]

[a] Department of Nuclear Engineering, Texas A&M University College Station, TX 77843, USA
[b] Department of Mathematics, Texas A&M University College Station, TX 77843, USA

Keywords:
Finite elements
Adaptive mesh refinement
Multigroup diffusion approximation
Reactor simulation

A B S T R A C T

Adaptive mesh refinement (AMR) has been shown to allow solving partial differential equations to significantly higher accuracy at reduced numerical cost. This paper presents a state-of-the-art AMR algorithm applied to the multigroup neutron diffusion equation for reactor applications. In order to follow the physics closely, energy group-dependent meshes are employed. We present a novel algorithm for assembling the terms coupling shape functions from different meshes and show how it can be made efficient by deriving all meshes from a common coarse mesh by hierarchic refinement. Our methods are formulated using conforming finite elements of any order, for any number of energy groups. The spatial error distribution is assessed with a generalization of an error estimator originally derived for the Poisson equation.

Our implementation of this algorithm is based on the widely used Open Source adaptive finite element library deal.II and is made available as part of this library's extensively documented tutorial. We illustrate our methods with results for 2-D and 3-D reactor simulations using 2 and 7 energy groups, and using conforming finite elements of polynomial degree up to 6.

1. Introduction

In many engineering disciplines, from structural mechanics to fluid dynamics, automated Adaptive Mesh Refinement (AMR) is now an established technique for obtaining numerical solutions with higher accuracy and resolution, while requiring less memory and shorter CPU times. Adaptivity, which can be traced back to the late 1970s (Babuška and Rheinboldt, 1978), is based on the idea that in order to achieve high accuracy, a uniformly fine mesh is not necessarily required; rather, the computational grid only needs to be fine in regions where the solution is rough and can be coarse in areas where the solution is smooth and, therefore, well resolved even on large cells. The challenge is that, in general, it is not known *a priori* where the solution will require the mesh to be fine. Consequently, the computation of local *error* or *smoothness indicators* from a numerical solution, previously obtained on a coarser mesh, lies at the heart of all adaptive mesh refinement algorithms, and a significant number of successful approaches have been developed for this problem in the last decade (Ainsworth and Oden, 2000; Bangerth and Rannacher, 2003; Babuška and Strouboulis, 2001; Braess and Verfürth, 1996). Using these methods, it has been shown for many problems that the computational effort needed to reach a certain accuracy can often be reduced by one or several orders of magnitude compared to uniform meshes, frequently enabling the solution of entire new classes of problems that were previously considered too computationally expensive to solve the required accuracy.

For a variety of reasons, AMR has not yet been widely used in nuclear science and engineering, with only a few references available in the literature (see our review below). Among the main causes is that the correct description of many processes in neutronics applications in nuclear engineering is the transport equation (Bell and Glasstone, 1970; Duderstadt and Martin, 1979), an equation that is extraordinarily complicated to solve numerically, even in the absence of advanced numerical methods like adaptivity. These complications arise from its hyperbolic character that allows discontinuous solutions and in particular its dependence on seven variables (three space dimensions, the two-dimensions of direction, time, and energy).

Consequently, a significant number of approximations have been developed to make it tractable for particular cases. For example, the multigroup diffusion approximation is often employed in 3-D reactor analysis and design (Covington, 1995; Lautard et al., 1990). This approximation leads to a collection of partial differential equations for individual energy groups that need to be solved concurrently. While adaptive mesh refinement techniques have been investigated for a wide variety of engineering

* Corresponding author.
E-mail addresses: yaqiwang@tamu.edu (Y. Wang), bangerth@math.tamu.edu (W. Bangerth), ragusa@ne.tamu.edu (J. Ragusa).

0149-1970/$ – see front matter © 2008 Elsevier Ltd. All rights reserved.
doi:10.1016/j.pnucene.2008.11.005

Please cite this article in press as: Wang, Y., et al., Three-dimensional *h*-adaptivity for the multigroup neutron diffusion equations, Prog. Nucl. Energy (2009), doi:10.1016/j.pnucene.2008.11.005

problems in the past, the multigroup approximation that arises in the treatment of the transport or diffusion equations has properties that require a re-analysis of straightforward approaches. Among its particularities is that, unlike most other coupled systems the authors are aware of, individual solution components are not necessarily smooth or rough in the same parts of the domain (see the numerical examples in Section 4 as well as those shown in Jatuff and Gho (1998)). This is easy to understand: fast particles typically travel relatively unimpeded through fine-scale features of the medium and their spatial distribution is therefore a relatively smooth function; on the other hand, thermal (slow) particles typically interact more locally and strongly with materials, and the resulting large variations of cross sections values and mean-free-path lengths then lead to less smooth solutions. Thus, it is not *a priori* clear that it is worthwhile to discretize different energy groups with a single mesh.

In this contribution, we propose and evaluate an automated mesh adaptation technique based on the use of arbitrary-order finite elements that is applied to the multigroup diffusion approximation. The main feature of this method is the use of separate and possibly differing meshes for individual energy groups. While in general the use of different meshes can lead to expensive algorithms, we will show how to efficiently use our approach by using meshes that are hierarchically refined from a common coarse grid. The spatial integration of terms that involve shape functions from different meshes can therefore be performed efficiently by considering only prolongations of shape functions from parent to child cell; this will be needed for group coupling terms such as scattering and fission events. We will illustrate this approach using *k*-eigenvalue benchmark problems taken from reactor analysis applications. We will present our algorithms and demonstrate their advantages over uniformly refined meshes using two 2-D 2-group examples as well as a 3-D 7-group example of significant complexity.

Our implementation of these algorithms is freely available as part of the widely used Open Source finite element library deal.II (Bangerth et al., 2007, 2008). The tutorial step-28 of deal.II contains the code developed in this present work; this tutorial is extensively documented and we explicitly encourage the use of this program as the basis for further experiments by other researchers. The results presented here use a slightly optimized but otherwise unchanged version of tutorial step-28. Since deal.II already provides most of the functionalities required for a project like this (including, for example, the handling of adaptive meshes, a variety of finite elements, all components of linear algebra, and input/output features), step-28 is in fact a relatively small code, of about 1200 lines of code, with several times that amount in documentation. Together with the extensive documentation of all aspects of deal.II (more than 5000 pages of API documentation along with more than 30 tutorial programs), we believe that step-28 is a good starting point for future research in this area.

We conclude this section by a brief review of the literature on adaptive mesh refinement for transport problems. For instance, Kanschat used fully adaptive finite approximations to the stationary, monochromatic radiative transfer problem (Richling et al., 2001; Kanschat, 1996) with mesh refinement driven by rigorously derived error estimates. Radiative transfer solvers are frequently coupled to AMR hydrodynamics codes, and consequently there has been a natural inclination to develop AMR capabilities for the transport/diffusion solvers as well. In Jessee et al. (1998), the gradient of the solution is employed to drive adaptive mesh refinement for the radiation transport component in 2-D Cartesian geometries for 1-group (one-frequency) equations. In Aussourd (2003), local a priori refinement techniques based on the value (or changes therein) of the neutron mean-free-path in a given cell are used for the 1-group transport equation in 3-D Cartesian geometries. While this approach takes into account the size of potential internal layers at a given location in the domain, it does not account for the *actual* smoothness of the solution at these locations and is therefore far from optimal; for example, in optically thick areas, the solution may well be approximated by a smooth spatial representation on coarse meshes despite the smallness of the mean-free-path. Klar et al. (2005) consider a coupled radiation-temperature model and apply adaptive methods to it that can resolve the boundary layer of a hot, homogeneous body that is in thermal contact with a cooler exterior.

In neutronics applications, Jatuff and coworkers (Jatuff, 1995; Jatuff and Gho, 1998) proposed error estimators applied to nodal diffusion equations. These estimators are based on the norm of the residual; they are related to the ones we use in the current contribution but do not have the correct scaling with powers of the mesh size. Zhang and Lewis (2001) presented a *p*-refinement technique (adaptive selection of the polynomial approximation) for the inter-element approximation in a primal hybrid finite element technique. Results were given for a 2-D 1-group diffusion problem; later they expanded the technique to the 2-D 1-group P_N equations (Zhang and Lewis, 2002). More recently, Wang and Ragusa applied the *hp*-adaptation concept to the multigroup diffusion equations, where both the local polynomial degree of shape functions and the local cell size are selected adaptively (Wang and Ragusa, 2006, in press). Error estimators for the combined *hp* adaptation are less mature and, as a consequence, these authors used the difference between a finer mesh solution Φ_{fine} and a coarser mesh solution Φ_{coarse} to drive the refinement (Demkowicz, 2006), with an overhead due to the computation of a fine solution at each step of the adaptation. Their results included mesh adaptation for 1-D multigroup and 2-D 1-group diffusion problems. Finally, the authors of (Ragusa, 2004, 2008) employed an error indicator based on estimating the second derivatives of the numerical solution and applied the resulting method to 1-group and 2-group diffusion applications. The error indicator used there is based on the interpolation error of linear finite elements (Gago et al., 1983). We will use a similar technique herein also for higher polynomial approximations; alternative methods for polynomial shape functions of degree p may use the tensor of $p+1$st derivatives of the numerical solution (see the general discussion in The deal.II manual and application in Leicht and Hartmann (2007) to the simulation of aerodynamic flows).

An outline of the remainder of this contribution is as follows: In Section 2, we briefly introduce the mathematical formulation used for the multigroup diffusion approximation eigenproblem. Section 3 presents the discrete formulation upon which we base our finite element scheme, the error indicator used to select mesh cells for refinement, and the mesh refinement scheme. In particular we also discuss the specificities of having group-dependent meshes and how an implementation can be made efficient. Finally, in Section 4, 2-D and 3-D results are presented using 2-group and 7-group diffusion problems. We conclude in Section 5 and present an outlook on open problems and possible next steps.

2. Mathematical formulation

2.1. The steady state multigroup diffusion equations

The goal of this paper is the development of automated spatial adaptivity for the numerical solution of the multigroup neutron diffusion equations. These equations can be derived as the diffusion dominated limit of the neutron transport equation and by binning neutron energies into a finite number G of groups (Bell and Glasstone, 1970; Duderstadt and Hamilton, 1976). Such problems in nuclear engineering typically involve either a criticality search eigenproblem or a source-driven problem. Here, we

Please cite this article in press as: Wang, Y., et al., Three-dimensional *h*-adaptivity for the multigroup neutron diffusion equations, Prog. Nucl. Energy (2009), doi:10.1016/j.pnucene.2008.11.005

will only present the eigenproblem case; the source-driven case is generally simpler and can be dealt with using the same techniques.

For conciseness, let us consider the neutron flux $\phi_g(\mathbf{r})$, $1 \le g \le G$ in the G different energy groups. In the absence of external neutron source, these satisfy the balance equations

$$-\nabla\cdot\Big(D_g(\mathbf{r})\nabla\phi_g(\mathbf{r})\Big) - \Sigma_{r,g}(\mathbf{r})\phi_g(\mathbf{r}) = \sum_{g'\neq g}\Sigma_{s,g'\to g}(\mathbf{r})\phi_{g'}(\mathbf{r})$$

$$\rho + \frac{\chi_g}{k_{\text{eff}}}\sum_{g'=1}^{G}\nu\Sigma_{f,g'}(\mathbf{r})\phi_{g'}(\mathbf{r}) \quad \mathbf{r}\in\Omega, 1\le g\le G. \tag{1}$$

The various coefficients in these equations have the following meaning:

- $D_g(\mathbf{r})$ is the diffusion coefficient in group g;
- $\Sigma_{r,\,g}(\mathbf{r})$ is the removal cross section in group g;
- $\Sigma_{f,\,g}(\mathbf{r})$ is fission cross section in group g, ν is the number of neutrons emitted per fission event, and χ_g is the fission spectrum. The quantity $S_f(\mathbf{r}) = \sum_{g'=1}^{G}\nu\Sigma_{f,g'}(\mathbf{r})\phi_{g'}(\mathbf{r})$ is often referred to as the fission integral;
- $\Sigma_{s,\,g\to g}^{'}$ is the scattering cross section from group g' to group g.

The equations above are augmented by Dirichlet boundary conditions $\phi_g = 0$ on the exterior boundaries of the domains we consider in Section 4 and boundary conditions $\mathbf{n}\cdot\nabla\phi_g = 0$ on planes of symmetry since we only consider one quadrant of a full reactor in our examples.

2.2. The eigenvalue problem

Considering all energy groups at once, we can re-write equation (1) in the following operator form:

$$(L-X)\phi = \frac{F}{k_{\text{eff}}}\phi \tag{2}$$

where L, X, and F are the loss, scattering, and fission operators, respectively. L here includes both the leakage and removal terms. Note that L is symmetric, whereas F and X are not. The multiplicative factor k_{eff} is the largest (and unique) eigenvalue of the operator $(L-X)^{-1}F$ (Krein–Rutman theorem, (Krein and Rutman, 1962)).

The goal of this paper is to solve the above k-eigenvalue problem using spatial adaptivity. Our numeric implementation uses the power method with Chebyshev acceleration (Ferguson and Derstine, 1977). The basic algorithm for this is as follows:

(1) Initialize the multigroup fluxes and the eigenvalue with $\phi_g^{(0)}$, $k_{\text{eff}}^{(0)}$; compute the initial fission integral $S_f^{(0)} = \sum_{g=1}^{G}\nu\Sigma_{f,g}(\mathbf{r})\phi_g^{(0)}(\mathbf{r})$ and set the iteration index to $n=1$.
(2) Solve for the multigroup fluxes $\phi_g^{(n)}$, $g=1,\ldots,G$ using

$$-\nabla\cdot D_g\nabla\phi_g^{(n)} + \Sigma_{r,g}\phi_g^{(n)} = \sum_{g'\neq g}\Sigma_{s,g'\to g}\phi_{g'}^{(n)} + \frac{\chi_g}{k_{\text{eff}}^{(n-1)}}S_f^{(n-1)}. \tag{3}$$

Without scattering of particles from lower energy to higher energy groups the above system is lower triangular in energy groups. When upscattering is present, the linear system is no longer triangular and an additional iterative loop is needed to solve for the thermal fluxes.

(3) Update the fission integral: $S_f^{(n)}(\mathbf{r}) = \sum_{g'=1}^{G}\nu\Sigma_{f,g'}(\mathbf{r})\phi_{g'}^{(n)}(\mathbf{r})$.
(4) Update the eigenvalue: $k_{\text{eff}}^{(n)} = \int_\Omega S_f^{(n)}(\mathbf{r}) / \int_\Omega S_f^{(n-1)}(\mathbf{r})k_{\text{eff}}^{(n-1)}$.
(5) Compare $k_{\text{eff}}^{(n)}$ with $k_{\text{eff}}^{(n-1)}$ and $\phi^{(n)}$ with $\phi^{(n-1)}$. If the changes are greater than a prescribed tolerance, then set $n=n+1$ and repeat the iteration starting at step-2; otherwise end the iteration.

We implement this algorithm to solve for the multiplication factor k_{eff} and the associated fundamental mode using the adaptive finite element scheme described in the following sections.

3. *h*-Adaptivity for the multigroup diffusion equations

Before describing our spatially adaptive algorithm, let us first consider the question whether it is adequate to solve for the fluxes ϕ_g of *all* energy groups $g=1,\ldots,G$ on the *same* mesh T, or whether it would be more appropriate to discretize each flux ϕ_g on its own mesh T_g. To this end, it is important to realize that a single mesh T can only be suitable for resolving all solution components ϕ_g simultaneously to equal accuracy if it is fine wherever at least one of these functions is non-smooth. If all components are non-smooth to the same degree in the same locations, then a single mesh is adequate. On the other hand, if the components ϕ_g have different degrees of variability in the same parts of the domain, or if they are non-smooth in different parts of the domain, then a single mesh would either be too fine in some areas for some of the components and consequently the mesh would be wasteful and lead to unnecessarily many degrees of freedom; or, alternatively, the mesh would be too coarse in some areas for at least some of the components and not yield appropriate accuracy uniformly for all components.

As will become obvious by looking at images of the individual components of solutions in Section 4, multigroup diffusion problems fall in the second category. In particular, it is physically obvious that fast neutrons tend to travel farther (due to smaller cross sections) and are, therefore, less affected by local variations in the material properties, whereas thermal neutrons "see" more localized details. Hence, smoother solutions are usually expected for higher energy neutrons and more rapidly varying solutions for lower energy neutrons. We can therefore expect that meshes that are adjusted to each energy group solution are significantly more efficient than using a single mesh for all groups.

The use of separate meshes for different energy groups has two principal consequences for their efficient implementation. First, we need to find a way to refine the meshes individually. Secondly, when assembling the cross-group source terms (fission and scattering) in the power iteration, we have to integrate the solution $\phi_{g'}^{(n)}$ defined on mesh $T_{g'}$ against the shape functions defined on mesh T_g. We will discuss efficient algorithms for these tasks below, following a concise statement of the finite element discretization we use.

3.1. Discrete formulation

In order to discretize the nth power iteration of the eigenvalue problem of Eq. (1), we approximate $\phi_g^{(n)}$ by expanding it with respect to a set of N_g finite element shape functions $\phi_g^i(\mathbf{r})$ defined on meshes T_g, $g=1,\ldots,G$, yielding $\phi_{g,h}^{(n)}(\mathbf{r}) = \sum_{i=1}^{N_g}\Phi_{g,i}^{(n)}\varphi_g^i(\mathbf{r})$, see Brenner and Scott (2002), Braess (1997), Carey and Oden (1984). The coefficients $\Phi_{g,i}^{(n)}$ are the unknowns to be solved for. For lowest-order (linear) continuous elements, shape functions are associated with the vertices of the mesh T_g. However, below we will also use higher order shape functions up to polynomial degree 6 that are associated with the faces, the edges, and the interior of cells. In the following sections, we will only consider meshes that consist of quadrilaterals (in 2-D) and hexahedra (in 3-D); however, all algorithms are readily applicable to triangular or tetrahedral elements as well.

Please cite this article in press as: Wang, Y., et al., Three-dimensional *h*-adaptivity for the multigroup neutron diffusion equations, Prog. Nucl. Energy (2009), doi:10.1016/j.pnucene.2008.11.005

Using a Galerkin procedure to determine the coefficients $\Phi_{g,i}^{(n)}$, we arrive at the following weak discrete form of 3, which we obtain by multiplying that equation by test functions φ_g^j, integrating over the spatial domain Ω, and integrating by parts all terms involving second derivatives:

$$\left(D_g\nabla\phi_{g,h}^{(n)},\nabla\varphi_g^j\right)+\left(\Sigma_{r,g}\phi_{g,h}^{(n)},\varphi_g^j\right) = \sum_{g'\neq g}\left(\Sigma_{s,g'\to g}\phi_{g',h}^{(n)},\varphi_g^j\right)+\left(\chi_g\bar{S}_f^{(n-1)},\varphi_g^j\right). \quad (4)$$

Here, $(u,v)=\int_\Omega u(\mathbf{r})v(\mathbf{r})d^3r$. Since this has to hold for each of the test functions φ_g^j, $j=1,\ldots,N_g$, $g=1,\ldots,G$, we obtain a system of linear equations for the coefficients $\Phi_{g,i}^{(n)}$ that can be solved using a preconditioned conjugate gradient solver, owing to its symmetry and positive definiteness.

Instead of going into the technical details of the other steps of the iterative procedure to compute k_{eff}, which were outlined in Section 2.2 and are detailed in Wachspress (1966) for instance, we will focus on the implications of automatically choosing adaptive meshes in the remainder of this section.

3.2. Outer mesh iteration

In adaptive mesh refinement algorithms, one usually starts with a coarse mesh in order to compute a rough approximate solution. This solution is then used to compute a refinement indicator that states on which cells the error is likely to be the largest. The cells with the largest error are then refined, those with the smallest error are coarsened, and the solution procedure starts over on this new mesh. The mesh adaptation iteration proceeds until we are satisfied with the accuracy of the solution. Since each mesh has more cells than the previous one, the total compute time is usually dominated by computations on the last mesh. The additional effort necessary to achieve a well-chosen mesh for a given accuracy (i.e., computing solutions and refinement indicators on coarser meshes) is, therefore, not a large factor in adaptive mesh calculations.

For the present problem, we solve the entire eigenvalue problem on one set of meshes T_g^m, $g=1,\ldots,G$, where m denotes the mesh iteration number. We then compute refinement indicators $\eta_{g,K}$ for all cells $K\in T_g^m$. With these indicators, we refine the mesh T_g^m to obtain the next mesh T_g^{m+1}. The final solution $\phi_{g,h}^{(n)}$ on the old mesh T_g^m is interpolated to the new mesh to obtain the initial guess $\phi_{g,h}^{(0)}$ for the power iteration procedure on the next set of meshes, T_g^{m+1}.

Because all following discussions will only concern a single set of meshes, we will drop the mesh iteration index m in the remainder of this paper, except where ambiguous.

3.3. Mesh refinement

The central component of the mesh iteration is the estimation of the error on each cell K of each of the meshes T_g^m, $g=1,\ldots,G$, in order to obtain refinement and coarsening criteria. Such error indicators are ideally derived using *a posteriori* error estimators using strict upper bounds on the total error (Ainsworth and Oden, 2000). For the current nonlinear eigenvalue problem 2, strict estimates or error approximations could be derived using the techniques discussed in Bangerth and Rannacher (2003); however, they would be complicated to implement and expensive to evaluate, requiring the solution of a second problem and the evaluation of a significant number of primal and dual residual terms on each cell.

On the other hand, experience has shown that oftentimes it is sufficient to have *error indicators* to drive mesh refinement. Such indicators typically determine the smoothness of a solution, by computing estimates of higher order derivatives. In our calculations, we use an indicator that uses the formula derived by Kelly et al. in Gago et al. (1983). In that paper, an *a posteriori* error estimator is derived for the Poisson equation; it approximates the error per cell by integrating the jump of the gradient of the solution along the faces of each cell, i.e., by computing

$$\rho_{g,K}=\sqrt{h_K}\left\|\left[n\cdot\nabla\phi_{g,h}^{(n)}\right]\right\|_{\partial K},$$

where h_K is the diameter of cell $K\in T_g$, $g=1,\ldots,G$. ∂K represents the edges in 2-D or the faces in 3-D of cell K, and $\mathbf{n}$ is the normal unit vector on ∂K. This quantity is equivalent to the norm of the second derivatives of a function, up to a power of h_K. While the expression was derived as an error *estimator* for the Poisson equation, it is widely used as a heuristic refinement *indicator* in many other applications as well and is considered a good choice in the absence of actual estimators for a particular equation (see, for example, (Bangerth and Joshi, 2008; Bangerth, 2008; Kirk and Carey, 2008)). It is also implemented in a number of standard finite element software packages (Bangerth et al., 2007, 2008; Kirk et al., 2006). The obvious generalization of the indicator above to cases where the diffusion operators contains a non-constant diffusion coefficient is to use the jump of net current,

$$\rho_{g,K}=\sqrt{h_K}\left\|\left[D_g n\cdot\nabla\phi_{g,h}^{(n)}\right]\right\|_{\partial K}.$$

This is the form that we will use in our numerical experiments below.

The next question is how to use these indicators to refine the cells of all the triangulations T_g. In general, it needs to be understood that the quantities $\rho_{g,K}$ only indicate the magnitude of the second derivative of the solution component ϕ_g at the location of cell K, and thereby presumably the magnitude of the local error $\phi_g-\phi_{g,h}$. However, $\rho_{g,K}$ does not contain any information regarding the quantity of interest (for example the eigenvalue k_{eff}) that drives the numerical solution, or, in other words, why it is important to have a small local error on cell K. For example, in 2-group diffusion problems, the fast flux is about one order of magnitude larger than the thermal flux; if the solutions would otherwise have similar qualitative behavior, then the indicators $\rho_{g,K}$ would also be ten times larger for the fast neutron flux. However, this does not mean that the fast group mesh should be preferentially refined: suppose, for example, that the quantity we are interested in is the power distribution – a quantity mostly driven by thermal neutrons in light water reactors due to the significantly higher thermal cross sections – then refinement of the thermal group mesh is clearly of importance as well.

A good error indicator would therefore multiply the smoothness indicator $\rho_{g,K}$ by an importance factor $z_{g,K}$ to obtain refinement indicators $\eta_{g,K}=\rho_{g,K}z_{g,K}$. Such importance factors can be computed using duality techniques (Bangerth and Rannacher, 2003), however at the price of a significant mathematical and computational overhead. In this contribution, we do not intend to describe such a theory and instead will choose the importance factors heuristically as $z_{g,K}=(\|\phi_{g,h}^{(n)}\|_{L^\infty(\Omega)})^{-1}$, thereby ensuring equal weight for all energy groups. An alternative choice we have investigated is $z_{g,K}=\|\Sigma_{f,g}\|_{L^\infty(K)}$ (i.e., the magnitude of the fission cross section on each cell), a choice suggested by the importance with which ϕ_g appears in the fission integral that is employed in the computation of k_{eff}; however, despite the fact that it makes intuitive sense, this choice does not lead to an efficient refinement indicator and performs significantly worse than the simple choice above in numerical experiments, mostly due to the fact that regions containing no fissile materials, such as reflector zones, are not considered for refinement with this alternate choice.

Please cite this article in press as: Wang, Y., et al., Three-dimensional *h*-adaptivity for the multigroup neutron diffusion equations, Prog. Nucl. Energy (2009), doi:10.1016/j.pnucene.2008.11.005

Using above definition for our refinement indicators $\eta_{g,K}$, we refine a mesh cell K if

$$\eta_{g,K} > \alpha_1 \max_{1\le g\le G,\ K\in T_g} \eta_{g,K} \tag{5}$$

and coarsen it if

$$\eta_{g,K} < \alpha_2 \max_{1\le g\le G,\ K\in T_g} \eta_{g,K}. \tag{6}$$

In the numerical experiments shown in Section 4, we use $\alpha_1 = 0.3$ and $\alpha_2 = 0.01$.

An interpretation of this strategy is that if for a given energy group g there are many cells $K\in T_g$ for which the refinement indicators are large, due to roughness in the solution or large importance factor, then many cells will be above the refinement threshold and will be selected for refinement. On the other hand, if there are a few cells with large errors and many cells with small errors, for example because the solution is overall rather smooth except at a few places, then only the few cells with large refinement indicators will be refined. Finally, if the solution for a given energy group is smooth everywhere, then none of its cells will be refined until the refinement indicators for cells on the meshes of other energy groups have been sufficiently reduced by mesh refinement. Consequently, the strategy allows for meshes that track the global smoothness properties of the solutions of *all* energy groups equally well.

3.4. Assembling terms on different meshes

A consequence of using different meshes for different energy groups is that in the discrete counterpart of step-3 of the eigenvalue iteration, i.e., in equation (4), we have to compute a right hand side vector that contains terms of the following form:

$$F_i = \int_\Omega f(\mathbf{r})\phi^{(n)}_{g',h}(\mathbf{r})\varphi^i_g(\mathbf{r})d^3r, \tag{7}$$

where $f(\mathbf{r})$ is one of the coefficient functions $\Sigma_{s,\,g'\to g}$ or $\chi_g\nu\Sigma_{f,\,g'}$ used in the right hand side of the eigenvalue equation. $\varphi_{g'}$ can be expanded as $\phi_{g',h}(\mathbf{r}) = \sum_j \Phi^j_{g'}\varphi^j_{g'}(\mathbf{r})$, with basis functions $\varphi_{g'}{}^j(\mathbf{r})$. Consequently, the contribution to the right hand side can be written as

$$F_i = \sum_{j=1}^{N_{g'}} \left\{ \int_\Omega f(\mathbf{r})\varphi^i_g(\mathbf{r})\varphi^j_{g'}(\mathbf{r})d^3r \right\} \Phi^j_{g'}. \tag{8}$$

Note that the test functions $\varphi_g(\mathbf{r})$ are defined on mesh T_g, whereas the basis functions $\varphi'_g(\mathbf{r})$ are defined on mesh $T_g{}'$. Hence, it is not possible to simply split the integral over Ω into integrals over the cells of either mesh g or g'.

In general, integrating terms that involve functions defined on two entirely different meshes is an expensive procedure, since it involves finding the cell of one mesh in which a quadrature point defined on the other mesh lies. The integration will in this case have a complexity higher than $O(N)$, i.e., the number of operations will grow faster than linearly with the number of cells N. However, as we will show in the following, this problem can be avoided if we use *hierarchical* meshes that all result from regular refinement of the same initial coarse mesh. In that case, we assume that all energy groups start out with the same coarse mesh, i.e., $T^0_g = T_{g'}{}^0$, and that we refine a mesh by regular bisection of cells (i.e., quadrilaterals in 2-D are subdivided into four child-cells whereas hexahedra in 3-D yield eight child-cells). In the rest of this section we present an algorithm that retains optimal order complexity (i.e., its compute time and memory are linear in the number of cells) and that to our knowledge has not been presented before in the finite element literature.

The algorithm rests on the observation that cells on each of the two grids remain related despite different refinement histories and that we can always find a set of cells, which we denote by $T_g \cap T_g{}'$, that satisfy the following conditions:

- the union of the cells covers the entire domain, and
- a cell $K\in T_g \cap T_g{}'$ is active on at least one of the two meshes.

Here, we denote a cell as *active* if it is not refined any further, i.e., it is a cell on which shape functions are defined. A cell becomes inactive after it is refined.

A way to construct this set of cells is to take each cell of the coarse mesh and do the following steps: (i) if the cell is active on either T_g or $T_g{}'$, then add this cell to the set; (ii) otherwise, i.e., if this cell has children on both meshes, then do step (i) for each of the children of this cell. With this, we can write Eq. (8) as follows:

$$F_i = \sum_{K\in T_g\cap T_{g'}} F_i|_K,\ \ F_i|_K = \sum_j \left\{ \int_K f(\mathbf{r})\varphi^i_g(\mathbf{r})\varphi^j_{g'}(\mathbf{r})d^3r \right\} \Phi^j_{g'}. \tag{9}$$

By construction, there are now three cases to be considered:

(i) The cell K is active on both meshes, i.e., both the basis functions φ^i_g as well as $\varphi_g{}^{ij}$ are defined on K.
(ii) The cell K is active on mesh g, but not on mesh g', i.e., the φ^i_g are defined on K, whereas the $\varphi_g{}^{ij}$ are defined on children of K.
(iii) The opposite case, i.e., the cell K is active on mesh g', but not on mesh g.

To compute the right hand side contributions above, we need to consider each of these three cases separately:

(i) If the cell K is active on both meshes, then we can directly evaluate the integral since both sets of shape functions are defined on this cell.
(ii) If the cell K is active on mesh g, but not on mesh g', then the basis functions $\varphi^j_{g'}$ are only defined either on the children K_c, with $0\le c<2^{\dim}$, or on children of these children if cell K is refined more than once on mesh g'.

Let us assume that K is only refined once more on mesh g' than on mesh g. Using the fact that we use embedded finite element spaces where each basis function on one mesh can be written as a linear combination of basis functions on the next refined mesh, we can expand the restriction of φ^i_g to child cell K_c into the basis functions defined on that child cell (i.e., on cells on which the basis functions $\varphi^l_{g'}$ are defined):

$$\varphi^i_{g,h}|_{K_c} = \sum_l B^{il}_c \varphi^l_{g'}|_{K_c}. \tag{10}$$

B_c is the matrix that interpolates data from a cell to its c-th child cell. We then write the contribution of cell K to the right hand side component F_i as

$$\begin{aligned} F_i|_K &= \sum_j \left\{ \int_K f(\mathbf{r})\varphi^i_g(\mathbf{r})\varphi^j_{g'}(\mathbf{r})\mathrm{d}x \right\} \Phi^j_{g'} \\ &= \sum_j \left\{ \sum_{c=1}^{2^{\dim}} \sum_l B^{il}_c \int_{K_c} f(\mathbf{r})\varphi^l_{g'}(\mathbf{r})\varphi^j_{g'}(\mathbf{r})\mathrm{d}^3r \right\} \Phi^j_{g'}. \end{aligned}$$

In matrix notation, this can be written as

Please cite this article in press as: Wang, Y., et al., Three-dimensional *h*-adaptivity for the multigroup neutron diffusion equations, Prog. Nucl. Energy (2009), doi:10.1016/j.pnucene.2008.11.005

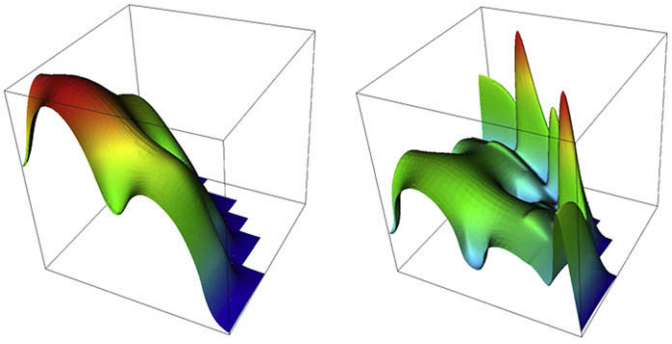

Fig. 1. Example 1: Solutions after 9 adaptive refinement iterations, fast group (left), thermal group (right), using quadratic finite elements.

$$F_i|_K = \sum_{c=1}^{2^{\dim}} F_i|_{K_c}, \quad F_i|_{K_c} = \sum_j \sum_l B_c^{il} M_{K_c}^{lj} \Phi_{g'}^j = \sum_j \left(B_c M_{K_c}\right)^{ij} \Phi_{g'}^j,$$

where $M_{K_c}^{lj} = \int_{K_c} f(\mathbf{r}) \varphi_{g'}^l(\mathbf{r}) \varphi_{g'}^j(\mathbf{r}) \mathrm{d}^3 r$ is the weighted mass matrix on child c of K.

On the other hand, if a child K_c of K is not active, then we have to apply the process recursively, i.e., we have to interpolate the basis functions φ_g^i onto child K_c of K, then onto child $K_{cc'}$ of that cell, onto child $K_{cc'c''}$ of that one, etc, until we find an active cell. We then have to sum all the contributions from all the children, grandchildren, etc, of cell K, with contributions of the form

$$F_i|_{K_{cc'}} = \sum_j \left(B_c B_{c'} M_{K_{cc'}}\right)^{ij} \Phi_{g'}^j, \tag{11}$$

or

$$F_i|_{K_{cc'c''}} = \sum_j \left(B_c B_{c'} B_{c''} M_{K_{cc'c''}}\right)^{ij} \Phi_{g'}^j, \tag{12}$$

etc. The matrix on the right can be computed by recursing into the hierarchy of cells generated by regular subdivision of cells.

(iii) The last case is where K is active on mesh g' but not mesh g. In that case, we have to express basis function $\varphi_{g'}^j$ in terms of the basis functions defined on the children of cell K, rather than φ_g^i as before. This of course works in exactly the same way. If the children of K are active on mesh g, then a similar procedure leads to the following expression:

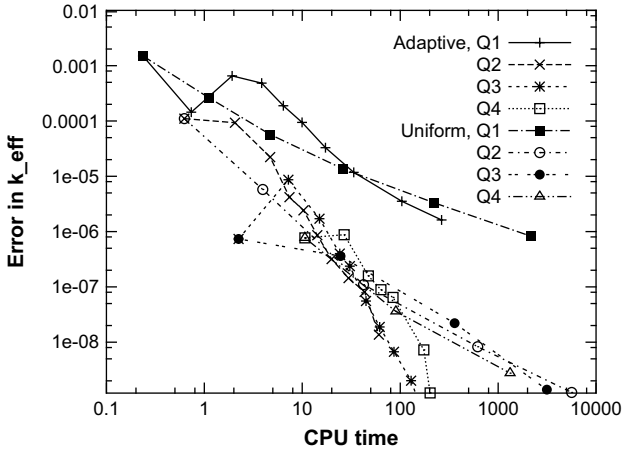

Fig. 2. Example 1: Accuracy in the eigenvalue k_{eff} as a function of CPU time for uniform and adaptive mesh refinement, for linear, quadratic, cubic, and quartic elements.

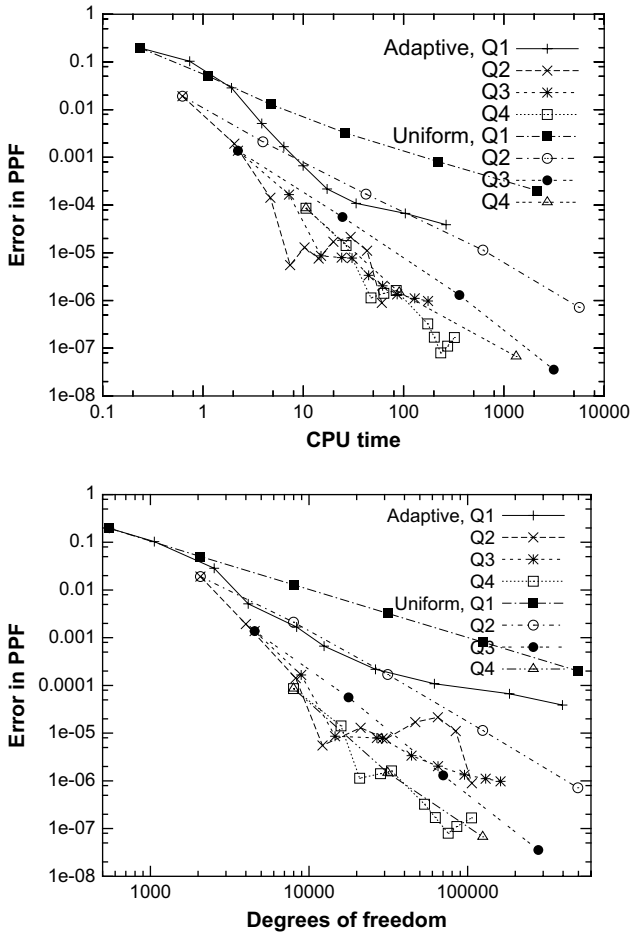

Fig. 3. Example 1: Accuracy in the core power peaking factor as a function of CPU time (top) and the number of unknowns (bottom) for uniform and adaptive mesh refinement, for linear, quadratic, and cubic elements.

$$F_i|_K = \sum_j \left\{ \int_K f(\mathbf{r}) \varphi_g^i(\mathbf{r}) \varphi_{g'}^j(\mathbf{r}) \mathrm{d}x \right\} \Phi_{g'}^j$$

$$= \sum_j \left\{ \sum_{c=1}^{2^{\dim}} \int_{K_c} f(\mathbf{r}) \varphi_{g'}^i(\mathbf{r}) B_c^{jl} \varphi_{g'}^l(\mathbf{r}) \mathrm{d}^3 r \right\} \Phi_{g'}^j.$$

In matrix notation, this expression now reads as

$$F_i|_K = \sum_{c=1}^{2^{\dim}} F_i|_{K_c}, \quad F_i|_{K_c} = \sum_j \sum_l M_{K_c}^{il} B_c^{jl} \Phi_{g'}^j = \sum_j \left(M_{K_c} B_c^T\right)^{ij} \Phi_{g'}^j, \tag{13}$$

and, correspondingly, for cases where cell K is refined more than once on mesh g:

$$F_i|_{K_{cc'}} = \sum_j \left(M_{K_{cc'}} B_{c'}^T B_c^T\right)^{ij} \Phi_{g'}^j, \tag{14}$$

or

$$F_i|_{K_{cc'c''}} = \sum_j \left(M_{K_{cc'c''}} B_{c''}^T B_{c'}^T B_c^T\right)^{ij} \Phi_{g'}^j, \tag{15}$$

etc. In other words, the process works in exactly the same way as before, except that we have to take the transpose of the

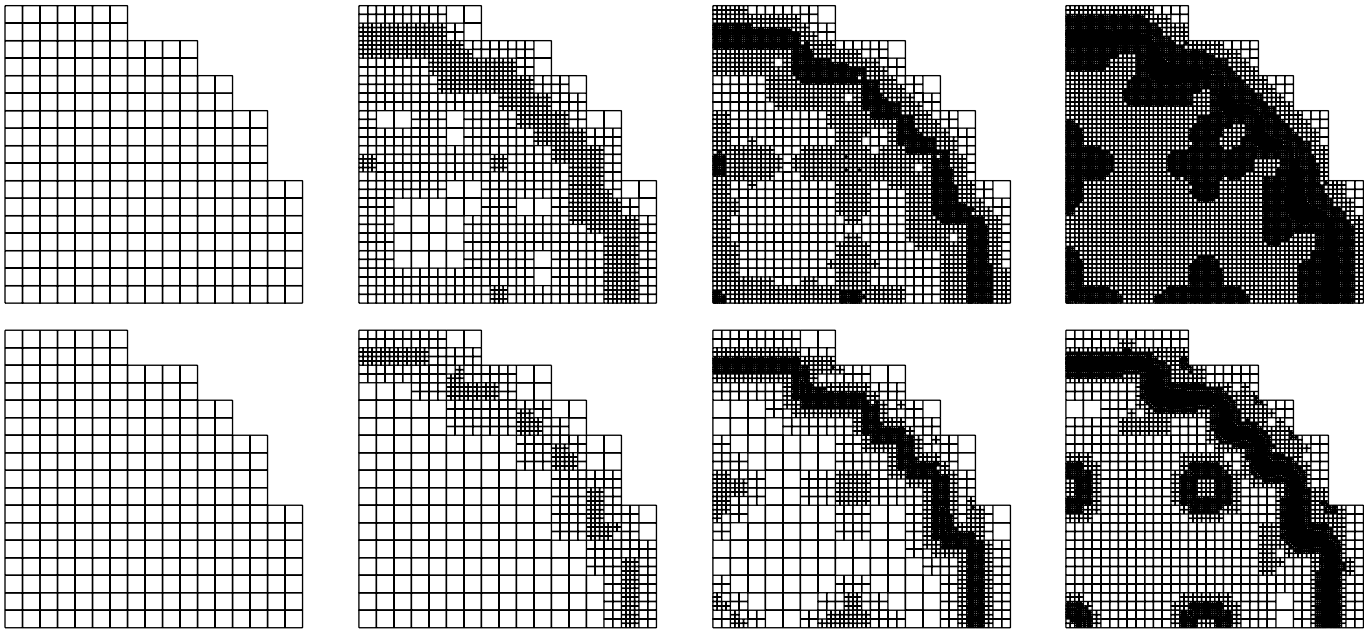

Fig. 4. Example 1: fast (top) and thermal (bottom) group meshes after 0, 2, 4 and 6 adaptive refinement iterations, using linear finite elements.

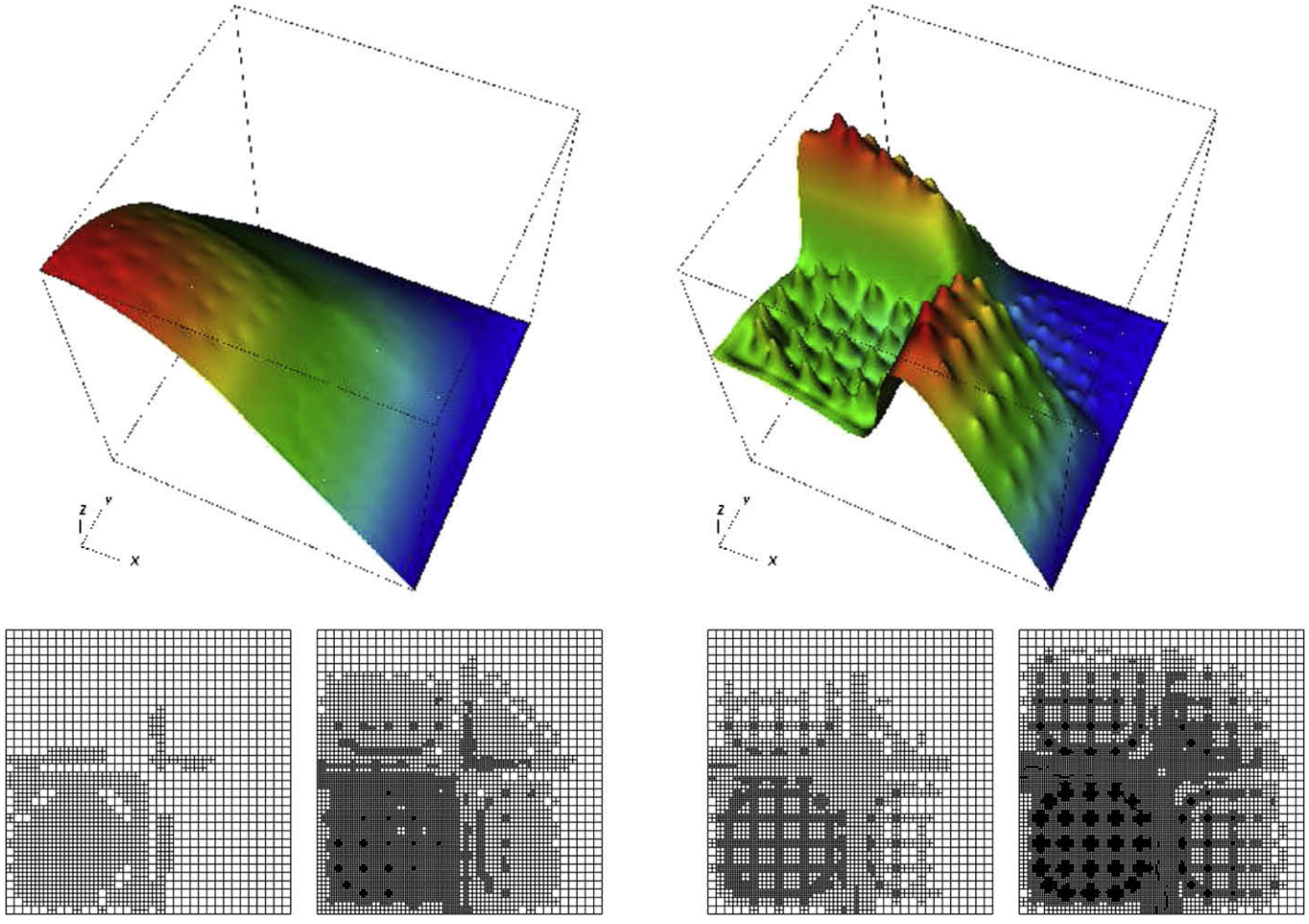

Fig. 5. Example 2: solutions of the 2-D 2-group multigroup neutron diffusion equations (top row; left: fast energy group $g = 1$, right: thermal energy group $g = 2$) and meshes after 2 and 4 adaptive refinement cycles (bottom row, left two panels: fast group; bottom row, right two panels: thermal group).

Please cite this article in press as: Wang, Y., et al., Three-dimensional *h*-adaptivity for the multigroup neutron diffusion equations, Prog. Nucl. Energy (2009), doi:10.1016/j.pnucene.2008.11.005

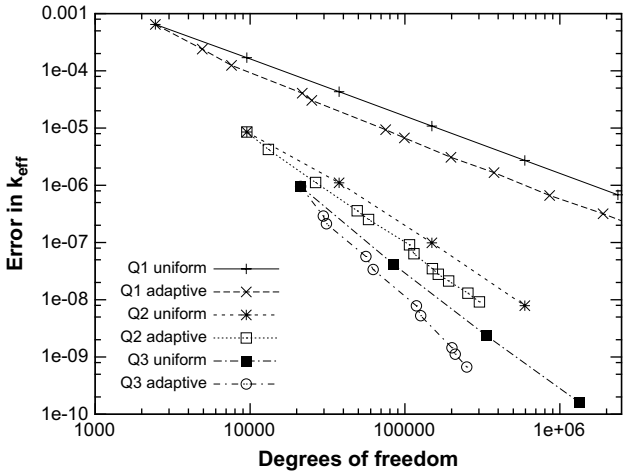

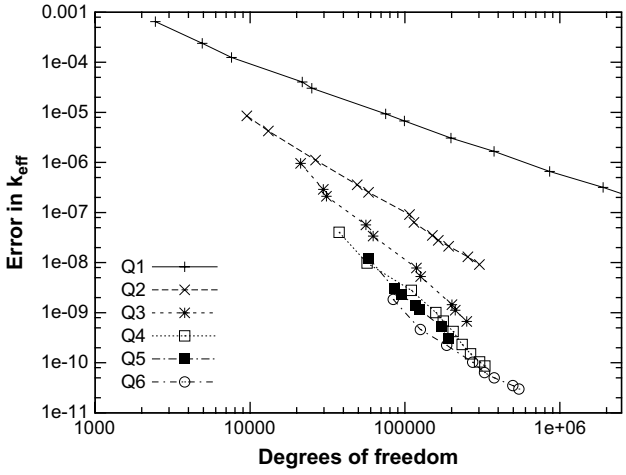

Fig. 6. Example 2: comparison of accuracy reached with a given number of unknowns for uniform and adaptive mesh refinement, for linear, quadratic, and cubic elements (top). Comparison of accuracy achieved with adaptive mesh refinement for elements of degree 1 through 6 (bottom).

prolongation matrices and need to multiply it to the mass matrix from the other side.

The expressions for cases (ii) and (iii) can be understood as repeatedly interpolating either the left or right basis functions in the scalar product $(f\varphi_g^i,\ \varphi_{g'}{}^j)_K$ onto child cells, and then finally forming the inner product (the mass matrix) on the final cell. To make the symmetry in these cases more obvious, we can write them as follows: for case (ii), we have

$$F_i|_{K_{cc'\cdots c(k)}} = \sum_j \left[B_c B_{c'} \cdots B_{c(k)} M_{K_{cc'\cdots c(k)}}\right]^{ij} \Phi_{g'}^j, \tag{16}$$

whereas for case (iii) we get

$$F_i|_{K_{cc'\cdots c(k)}} = \sum_j \left[\left(B_c B_{c'} \cdots B_{c(k)} M_{K_{cc'\cdots c(k)}}\right)^T\right]^{ij} \Phi_{g'}^j, \tag{17}$$

Although this process of computing terms that involve quantities defined on different meshes may appear cumbersome, it is easily implemented in a rather straightforward way using recursion and using the hierarchical structure of the meshes we use. In particular, we note that following from Eq. (9) the components $F_i = \sum_{K\in T_g \cap T_{g'}} F_i|_K$ of the right hand side vectors result from a sum of terms each of which is a linear function of the coefficients $\Phi_{g'}{}^j$, see equations (11–13). Consequently, we can write

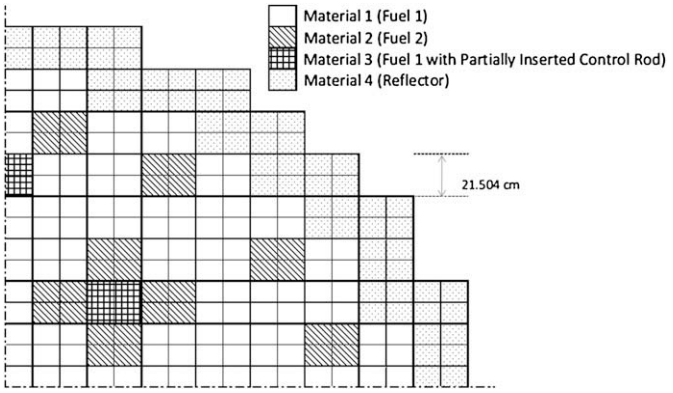

Fig. 7. Example 3: Core layout.

$$F = T_{gg'} \Phi_{g'} \tag{18}$$

where the (sparse) matrix $T_{gg'}$ is built using the techniques just described. In our implementation we build and store these matrices rather than re-assembling the terms on each cell in each power iteration, and F is then formed by a simple matrix-vector product; given the significant number of times we need to form vectors F this is more efficient. We will investigate this in Section 4.3.

4. Numerical results

In this section we present a number of numerical experiments that illustrate the approach we have described above. All computations were performed with a program based on the deal.II finite element library (Bangerth et al., 2008, 2007), an Open Source library that supports fully adaptive 1-D, 2-D, and 3-D meshes, a variety of different finite element types, and a large collection of classes supporting general finite element computations. An earlier version of the program used here has been extensively documented and will be distributed with next release of deal.II as step-28 of the tutorial.[1]

The test cases we will discuss below are: (1) the 2-D version of the 2-group IAEA PWR problem (Argonne Code Center, 1977), where data is given as piece-wise constant for each fuel assembly, (2) the C4 configuration of the 2-D 2-group pin-by-pin design of the OECD mixed oxide fuel benchmark (Lefebvre et al., 1996), where the data is piece-wise constant at the pin cell level, and (3) a 3-D 7-group problem with cross sections representative of UOX and MOX fuels and partial rod insertion.

In the following sections, we will compare results obtained on uniform and adaptively refined meshes with respect to (i) the accuracy of the eigenvalue k_{eff}, and (ii) the accuracy in the core power peaking factor. Here, we define the core power peaking factor as the maximum power produced *in each initial mesh cell* K_i, i.e.,

$$\text{PPF} = \max_{K_i} \frac{\int_{K_i} \sum_{g=1}^G \Sigma_{f,g}\phi_g}{\frac{1}{|\Omega|}\int_\Omega \sum_{g=1}^G \Sigma_{f,g}\phi_g}. \tag{19}$$

[1] Use of step-28 as the starting point for numerical experiments by others is possible and encouraged under the Open Source license of deal.II. We kindly request that all publications resulting from its use acknowledge the original authors, Yaqi Wang and Wolfgang Bangerth, as well as the creators of the deal.II library (Bangerth et al., 2007). The step-28 program differs from the one here only in that it does not use the Chebychev acceleration and it builds the cross-grid terms discussed in Section 3.4 on the fly in each iteration, whereas our final version caches some information for performance reasons.

Please cite this article in press as: Wang, Y., et al., Three-dimensional *h*-adaptivity for the multigroup neutron diffusion equations, Prog. Nucl. Energy (2009), doi:10.1016/j.pnucene.2008.11.005

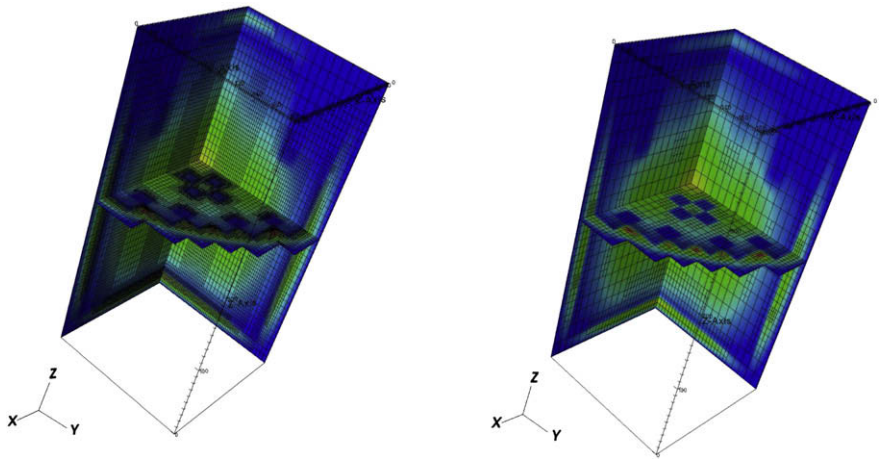

Fig. 8. Example 3: three-slice at $x = y = 0$ cm $z = 200$ cm of the Q_1 (left) and Q_2 (right) group-7 solutions and associated meshes after 7 and 2 adaptive mesh refinements, respectively.

It may seem that this definition, based on the initial cells favors uniform coarse meshes, in which errors may partially cancel out in through averaging. However, as we will show, this is in fact not the case, and adaptivity yields significantly more accurate results. Note that the initial meshes we will consider are based on the problem geometry (e.g., the core layout of fuel assemblies) and are typically used to output computed data such as power per assembly or quarter assembly; therefore, the power peaking factor above is not defined on an arbitrary set of cells but rather the fixed set of reactor blocks we are actually interested in.

4.1. Example 1: 2-D, two energy groups IAEA PWR benchmark

In this test, we use the 2-D version of the IAEA PWR benchmark (Argonne Code Center, 1977). The 2-D geometry consists of one quarter of a cross-sectional cut of the 3-D geometry at a height of $z = 200$ cm, in which four control rods are inserted. The initial mesh consists of square cells of 10 cm width (i.e., four cells per fuel assembly). We will present results obtained with uniform and adaptive refinement, for Lagrange elements of polynomial order 1 through 4. Fig. 1 shows the solutions for the two energy groups. It clearly shows that the solution for the fast group is significantly smoother than that for the thermal group, as well as the effect of the reflector layer on the outer rim of the reactor.

Fig. 2 shows the error in k_{eff} as a function of the CPU time required to compute it to a certain accuracy. For practical purposes, the eigenvalue must be obtained with at least 5 digits of accuracy (1 pcm) though for this particular case it is easy to approximate it to much higher accuracy. We computed the error in k_{eff} using a reference value obtained by extrapolating from a sequence of globally refined meshes using cubic polynomials. Comparing linear finite elements (Q_1) results, we observe that adaptive mesh refinement becomes competitive against uniform meshes in the 1-pcm range; for higher accuracy, e.g., 0.1 pcm, adaptive refinement with Q_1 elements is clearly superior than uniform mesh refinement. For higher order elements, adaptive refinement becomes competitive in the 0.1-pcm range as well.

Since the eigenvalue is a global quantity, it may not be too surprising to see that the benefits of adaptation are modest. Consequently, we also compare adaptive and uniform refinements for the core power peaking factor introduced above, a local quantity. Fig. 3 (top) shows the convergence in the peaking factor between the various refinement techniques as a function of CPU time. It is obvious that adaptive linear finite elements provide 1% accuracy five times faster than uniform refinement, and a 0.01% accuracy 20 times faster; for an accuracy of 0.01%, adaptive Q_1 elements are comparable to uniform Q_2 elements. Similarly, for higher finite elements, there is always a significant gain in accuracy of the power peaking factor when using mesh adaptation over uniform refinement. Similar gains can also be seen in Fig. 3 (bottom), where the convergence in the core power peaking factor is shown a function of the number of unknowns.

Meshes for Q_1 elements after no, 2, 4 and 6 adaptive refinements are shown in Fig. 4. From these images, it is clear that adaptive mesh refinement provides better results than uniform meshes: refinement occurs in regions of steep flux variations leading to a better numerical approximation, whereas regions of smooth solution do not require the same level of refinement. It is also worth mentioning that the same accuracy as obtained with Q_1 elements after six adaptive refinements is already reached with two refinements and Q_2 elements (see Fig. 3)

4.2. Example 2: 2-D, two energy groups, OECD-L-336 fuel assembly benchmark

As a second example, we consider a 2-D 2-group C4 configuration (semi-reflected MOX checker board) of the OECD/NEACRP L-336 mixed oxide fuel benchmark problem issued by the Organization for Economic Cooperation and Development/Nuclear Energy Agency Committee on Reactor Physics. We compare solutions using Q_p finite elements of polynomial degrees $p = 1$ through 6. In the initial mesh, each initial computational cell is equal to the homogeneous square fuel pin cell (i.e., an array of 34×34 cells). The meshes used for the fast and thermal energy groups are then refined according to the criteria discussed in Section 3.

We show the solutions of both groups as well as a succession of meshes used for the computations using Q_1 (i.e., bilinear) elements in Fig. 5. Even more so than in the first example, it is apparent that the solutions have entirely different smoothness properties: the fast group is relatively smooth, with only little dimples at the location of the guide tubes, while the thermal group shows large variations in neutron fluxes depending on the local neighborhood. On the other hand, the fast group flux is larger in magnitude by almost one order of magnitude. Thus, normalizing the group error estimators by the flux of each group proved to be important as it allows for an appropriate selection of the spatial zones and energy groups which require refinement, as can be seen by the level of refinement performed on the thermal flux in Fig. 5.

Please cite this article in press as: Wang, Y., et al., Three-dimensional *h*-adaptivity for the multigroup neutron diffusion equations, Prog. Nucl. Energy (2009), doi:10.1016/j.pnucene.2008.11.005

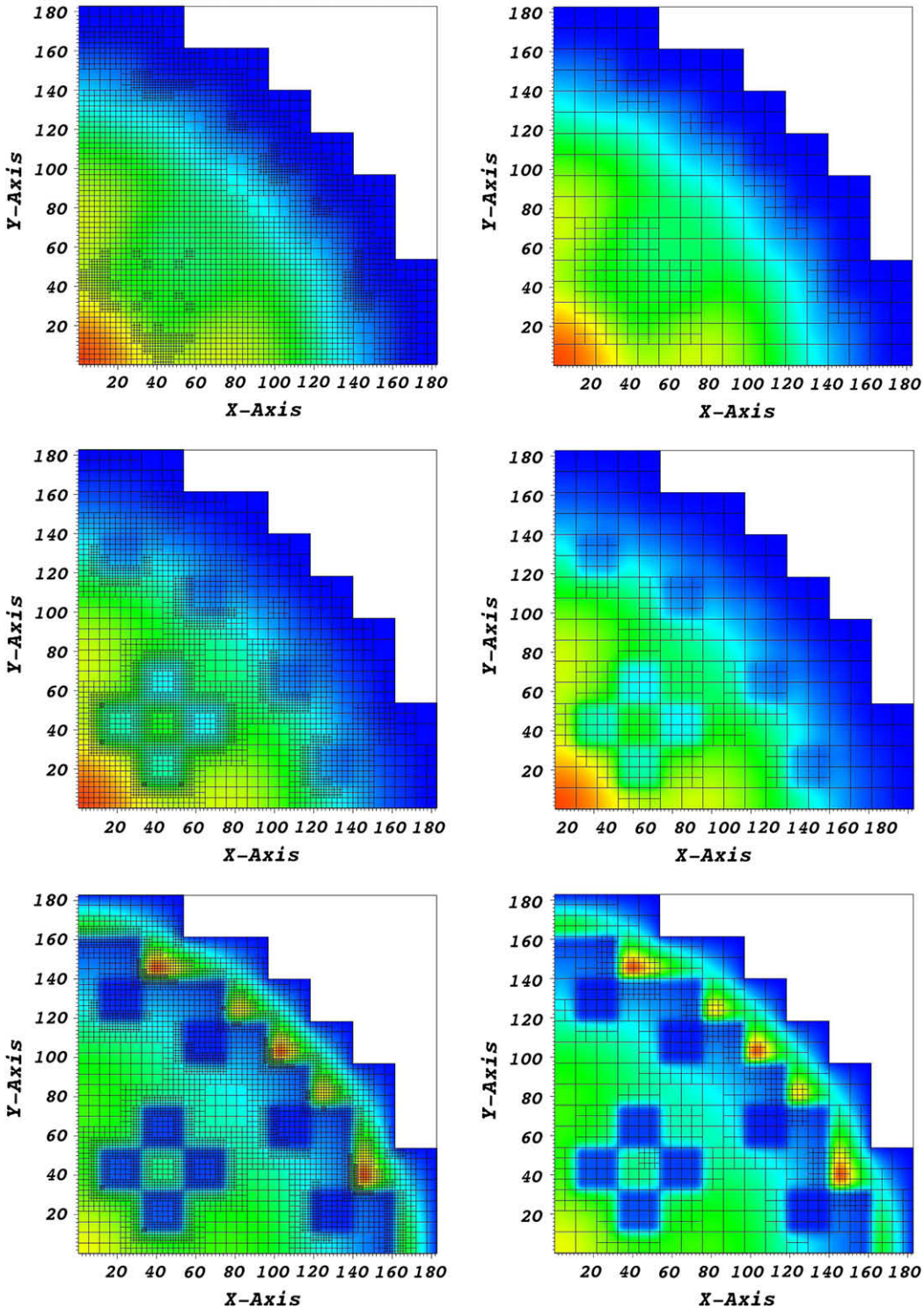

Fig. 9. Example 3: cross-section view at $z = 200$ cm of the Q_1 (left column) and Q_2 (right column) adapted meshes and solutions after 7 (left) and 2 (right) adaptive mesh refinements. Top row: group 1; middle row: group 5; bottom row: group 7.

In order to investigate if adaptive mesh refinement is indeed better than uniform meshes, the top panel of Fig. 6 shows a comparison of the convergence history for Q_1, Q_2, and Q_3 elements using both adaptive and uniform refinement. As can be seen from the figure, depending on the desired accuracy, adaptive meshes can achieve the same accuracy with up to 2–3 times fewer degrees of freedom as required for uniformly refined meshes. An alternative viewpoint is that adaptivity produces meshes on which the error is smaller by a factor of up to 10 for the same number of unknowns as on uniformly refined meshes. We observe similar savings by comparing the error with respect to CPU time rather than the number of degrees of freedom.

The bottom panel of Fig. 6 compares convergence of k_{eff} on adaptive meshes for elements Q_p of order $p = 1, 2, \ldots, 6$. As can be

Please cite this article in press as: Wang, Y., et al., Three-dimensional *h*-adaptivity for the multigroup neutron diffusion equations, Prog. Nucl. Energy (2009), doi:10.1016/j.pnucene.2008.11.005

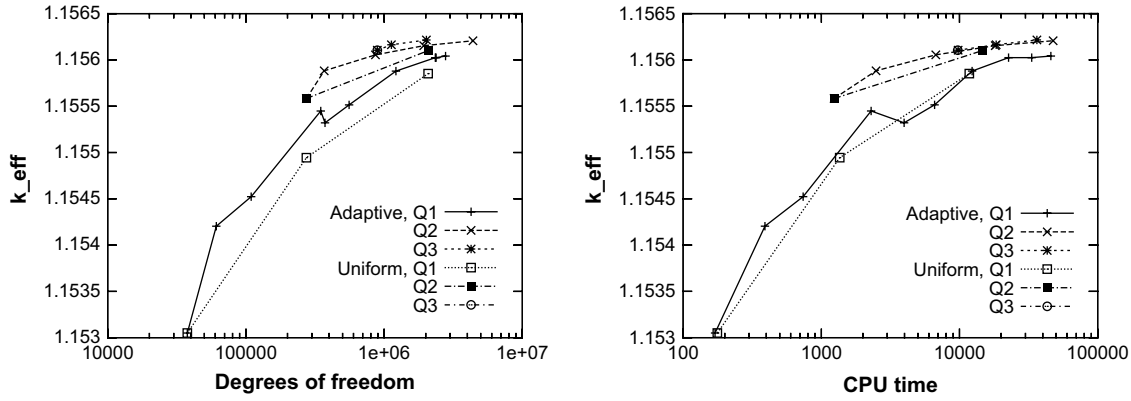

Fig. 10. Example 3: comparison of the eigenvalue k_{eff} as a function of the number of unknowns (left) and CPU time (right) for uniform and adaptive mesh refinement, for linear, quadratic, and cubic elements.

seen, the accuracy in the result can be increased significantly by choosing higher order finite elements up to $p = 4$. Beyond this, yet higher orders do not pay off any more. This should not be too unexpected given that the solution is rather rough at least for the thermal group.

4.3. Example 3: three space dimensions, seven energy groups

To conclude our series of tests, we consider a 3-D core, 7-group calculation. The core layout, composed of homogenized fuel assemblies, is given in Fig. 7. We have chosen to consider two distinct types of fuel, representative of a UOX fuel (labeled Material 1, see Fig. 7) and MOX fuel (Material 2). This results in different and rapidly varying spatial flux distributions in the lower energy range. Additionally, a control rod (Material 3) is partially inserted in the UOX fuel. A reflector (Material 4) surrounds the fissile core radially and axially. For simplicity, a unique reflector composition is employed. The square fuel assemblies have a width of 21.504 cm, the active core height is 3.6 m, with an additional 20 cm of reflector at both top and bottom extremities, for a total height of 4 m. The control rods are inserted from the top in 120 cm of five fuel assemblies (the 240 cm below them are made of Material 1). The initial mesh is composed of right prisms with a square base of width 10.752 cm and height of 20 cm. We list the material constants used for this test case in Appendix A.

Fig. 8 presents the group-7 solutions and adapted meshes for Q_1 and Q_2 finite elements. The plots are provided at refinement cycle 7 for Q_1 and cycle 2 for Q_2, for which the answers have approximately reached the same level of accuracy (see the discussion of Figs. 10 and 11 below). Fig. 9 shows cross sections of the solution and adaptive meshes for groups 1 (fastest neutron group), 5, and 7 (slowest group), obtained using Q_1 and Q_2 elements. Again, the Q_1 results are shown at mesh iteration 7 whereas the Q_2 results are for mesh iteration 2, both computations yielding about similar accuracies on these meshes. As in the previous examples, the solution shows significant differences in smoothness between the energy groups and has appreciable variation in particular for the slower energy groups with steep gradients in MOX fuel assemblies (higher absorption) and in the reflector.

Figs. 10 and 11 show convergence of k_{eff} and the core power peaking factor under mesh refinement. This test case, being three-dimensional and with a significant number of energy groups, is complicated enough that we were not able to compute k_{eff} or the core power peaking factor to enough digits to allow us to compute convergence rates; all plots therefore only show actual values of these quantities (rather than errors) though convergence is apparent visually and a qualitative comparison of different methods is obviously possible. As in previous experiments, linear finite elements performed modestly better with adaptive refinement regarding the accuracy in the eigenvalue (significant gains in memory but comparable CPU times); for a local quantity, such as the core power peaking factor, linear finite elements on adapted meshes are clearly superior than on uniform meshes, with memory and CPU time savings of about one order of magnitude for a given accuracy. For quadratic finite elements, the results are even more favorable: Within a couple of mesh adaptations the power peaking

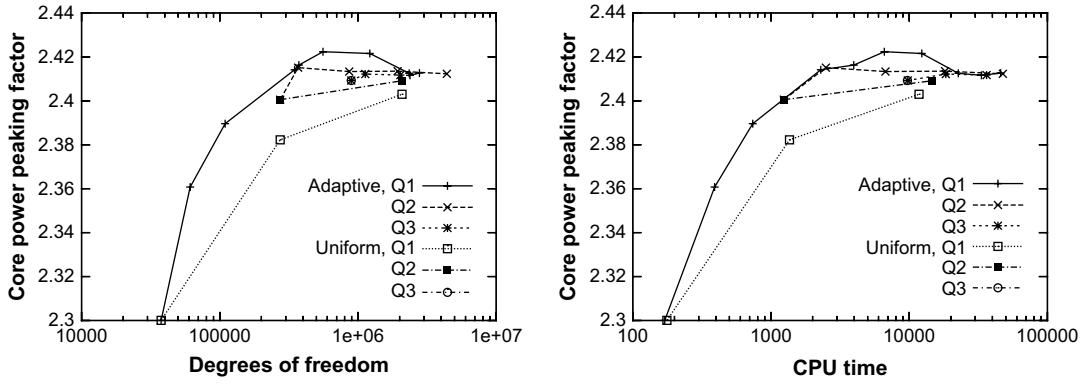

Fig. 11. Example 3: comparison of the core power peaking factor as a function of the number of unknowns (left) and CPU time (right) for uniform and adaptive mesh refinement, for linear, quadratic, and cubic elements.

Please cite this article in press as: Wang, Y., et al., Three-dimensional *h*-adaptivity for the multigroup neutron diffusion equations, Prog. Nucl. Energy (2009), doi:10.1016/j.pnucene.2008.11.005

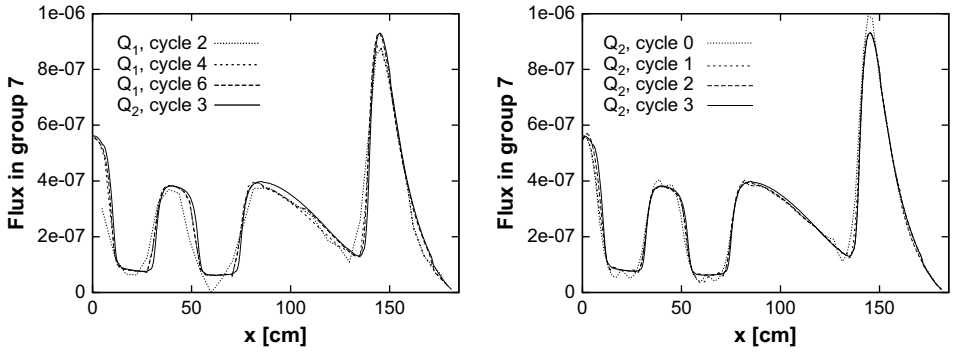

Fig. 12. Example 3: flux profile $\varphi_7(x, y = 39, z = 200)$. Left: Solution in adaptive refinement cycles 2, 4, 6, using Q_1 elements and as a reference solution cycle 3 of computations with Q_2 elements. Right: Solution in adaptive refinement cycles 0, 1, 2, and 3 using Q_2 elements.

factor appears converged, whereas the results obtained from Q_2 elements with one level of uniform refinement are still inaccurate. By extrapolating the results from the Q_2 initial and once-uniformly refined meshes, we can estimate that the twice-uniformly refined mesh would give results of the same accuracy level as the solution obtained from two mesh adaptations, but at a memory and CPU cost about 100 times larger; we have not been able to verify this in actual computations due to the excessive memory requirements of a twice globally refined mesh. As shown by the figure, Q_3 elements yield even higher accuracy at lower cost.

Finally, Fig. 12 shows the profile of the group-7 solution along the line $y = 39$ cm, $z = 200$ cm for several refinement cycles. The reference result utilizes Q_2 elements with 3 adaptive refinement cycles. From the left pane we can conclude that for Q_1 elements even after 6 adaptive cycle some discrepancies remain. On the other hand, from the right pane we infer that for Q_2 elements, after 2 adaptive cycles agreement with the reference solution is excellent.

Using this realistically sized test case we also investigated the cost associated with dealing with multiple meshes, rather than using a single mesh. To this end, we measured that only 2.5% of the total CPU time was spent on computing the transfer matrices $T_{gg'}$ discussed in equation (18) and that approximately 9.3% of the total CPU time was used in forming the right hand sides of the power iterations; not all of this time is of course caused by dealing with different meshes. Almost the entire rest of the CPU time was spent on solving the linear systems associated with power iterations. We conclude from this that the additional overhead for dealing with one mesh per energy group as compared to having a single mesh (adaptively or uniformly refined) is not very large and is easily offset by savings in the sizes of meshes adapted to individual energy groups.

5. Conclusions and outlook

In this contribution, we have presented an adaptive finite element algorithm for the multigroup diffusion approximation to the radiative transfer equation. It uses different meshes for each of the energy groups to resolve the smoothness properties of the solutions in each group. This approach is efficient because for this set of equations the smoothness of solution components varies greatly between energy groups, due to the significant variation in material parameters with energy.

Through a sequence of numerical experiments we have shown that the proposed algorithm performs better than uniformly refined meshes – in the most complicated three-dimensional case by orders of magnitude – and is therefore able to solve problems to accuracies previously impossible or to solve problems to the required accuracy for the first time at all.

Although we believe that the methods proposed here are a significant step forward, we are also of the opinion that it can be significantly extended and improved. Among these possibilities are:

- When implemented on a parallel computer with distributed memory, meshes have to be replicated on each machine anyway. This removes the additional (modest) memory requirements we currently impose on our computations by keeping G instead of only one mesh. The algorithms discussed in the current paper may therefore be even more efficient if implemented on distributed memory machines. The drawback of parallel implementations is, of course, that the eigensolver currently loops over energy groups in a sequential fashion, solving each one in turn.
- The choice of importance factor $z_{g,\ K}$ in Section 3.3 is heuristic. A proper importance factor can be derived by solving a dual problem (Bangerth and Rannacher, 2003) that computes the influence of a given cell K for a given group g on a target functional, for example the accuracy of the eigenvalue k_{eff}. For nonlinear problems like the current eigenvalue problem, the solution of such a dual problem only amounts to one additional power iteration step; nevertheless, the implementational burden would be significant. We believe that a properly computed weight factor should significantly increase the accuracy and reliability of adaptive approaches.
- Our approach of using several different grids can of course be applied also to some of the other approximations to the radiative transfer equation that result in a set of coupled partial differential equations. This includes, in particular, approaches like the P_N and SP_N methods.

Acknowledgments

Part of this research was funded through DOE grants DE-FG07-07ID14767 and DE-FG07-05ID14692. This publication is also partly based on work supported by Award No. KUS-C1-016-04, made by the King Abdullah University of Science and Technology (KAUST).

Appendix A

The following table lists the material parameters (cross sections) used for the 7-group example discussed in Section 4.3. Cross sections for the other two examples can be found in the references cited in the respective sections.

g	D^g	Σ_t^g	$\Sigma_s^{g\to1}$	$\Sigma_s^{g\to2}$	$\Sigma_s^{g\to3}$	$\Sigma_s^{g\to4}$	$\Sigma_s^{g\to5}$	$\Sigma_s^{g\to6}$	$\Sigma_s^{g\to7}$	$\nu\Sigma_f^g$	χ^g
Material 1											
1	1.9645058	0.0676314	0.1020466	0.0620793	0.0002150	0.0000011	0.0000000	0.0000000	0.0000000	0.0134820	0.5880000
2	0.9536659	0.0419533	0.0000000	0.3075751	0.0387120	0.0001802	0.0000139	0.0000022	0.0000003	0.0013607	0.4116600
3	0.6713391	0.0905403	0.0000000	0.0000000	0.4059798	0.0670154	0.0049246	0.0007649	0.0001458	0.0105424	0.0003400
4	0.6121584	0.2108010	0.0000000	0.0000000	0.0000000	0.3337204	0.1242644	0.0184459	0.0035045	0.0304014	0.0000000
5	0.7927936	0.1951705	0.0000000	0.0000000	0.0000000	0.0001053	0.2252836	0.1551156	0.0176976	0.0290938	0.0000000
6	0.5279811	0.2476514	0.0000000	0.0000000	0.0000000	0.0000000	0.0015182	0.3836842	0.1681179	0.1356622	0.0000000
7	0.2891938	0.2450183	0.0000000	0.0000000	0.0000000	0.0000000	0.0000000	0.0437284	0.9076112	0.3530487	0.0000000
Material 2											
1	1.9414176	0.0683040	0.1033918	0.0616757	0.0002144	0.0000011	0.0000000	0.0000000	0.0000000	0.0159816	0.5880000
2	0.9463810	0.0419533	0.0000000	0.3102656	0.0387188	0.0001802	0.0000139	0.0000022	0.0000003	0.0026033	0.4116600
3	0.6588437	0.0952487	0.0000000	0.0000000	0.4106882	0.0669145	0.0049246	0.0007649	0.0001458	0.0162543	0.0003400
4	0.5854027	0.2282893	0.0000000	0.0000000	0.0000000	0.3411193	0.1242039	0.0184459	0.0035045	0.0635115	0.0000000
5	0.6296201	0.2967373	0.0000000	0.0000000	0.0000000	0.0001396	0.2326825	0.1540596	0.0176976	0.0308870	0.0000000
6	0.3597307	0.5536969	0.0000000	0.0000000	0.0000000	0.0000000	0.0021774	0.3729222	0.1656292	0.6254627	0.0000000
7	0.2473365	0.4488244	0.0000000	0.0000000	0.0000000	0.0000000	0.0000000	0.0439369	0.8988671	0.7031916	0.0000000
Material 3											
1	1.8996137	0.0667524	0.1087219	0.0611430	0.0002033	0.0000010	0.0000000	0.0000000	0.0000000	0.0134820	0.5880000
2	0.9222381	0.0391507	0.0000000	0.3222889	0.0354180	0.0001643	0.0000127	0.0000020	0.0000003	0.0013607	0.4116600
3	0.6232103	0.0894575	0.0000000	0.0000000	0.4454075	0.0611758	0.0044825	0.0006961	0.0001326	0.0105424	0.0003400
4	0.5665006	0.2233427	0.0000000	0.0000000	0.0000000	0.3650651	0.1135291	0.0167962	0.0031905	0.0304014	0.0000000
5	0.7291666	0.2249611	0.0000000	0.0000000	0.0000000	0.0001071	0.2321818	0.1421733	0.0161370	0.0290938	0.0000000
6	0.4990789	0.2915378	0.0000000	0.0000000	0.0000000	0.0000000	0.0015247	0.3763592	0.1531972	0.1356622	0.0000000
7	0.2788687	0.3157843	0.0000000	0.0000000	0.0000000	0.0000000	0.0000000	0.0407812	0.8795214	0.3530487	0.0000000
Material 4											
1	2.6455026	0.0598000	0.0662000	0.0591000	0.0002830	0.0000015	0.0000000	0.0000000	0.0000000	0.0000000	0.0000000
2	1.1376564	0.0530000	0.0000000	0.2400000	0.0524000	0.0002500	0.0000192	0.0000030	0.0000004	0.0000000	0.0000000
3	1.1737089	0.1010000	0.0000000	0.0000000	0.1830000	0.0924000	0.0069400	0.0010800	0.0002060	0.0000000	0.0000000
4	1.1862396	0.2021000	0.0000000	0.0000000	0.0000000	0.0789000	0.1700000	0.0259000	0.0049300	0.0000000	0.0000000
5	0.9980040	0.2343000	0.0000000	0.0000000	0.0000000	0.0000373	0.0997000	0.2070000	0.0245000	0.0000000	0.0000000
6	0.5889282	0.2490000	0.0000000	0.0000000	0.0000000	0.0000000	0.0009170	0.3170000	0.2390000	0.0000000	0.0000000
7	0.2849003	0.0700000	0.0000000	0.0000000	0.0000000	0.0000000	0.0000000	0.0498000	1.1000000	0.0000000	0.0000000

References

Ainsworth, M., Oden, J.T., 2000. A Posteriori Error Estimation in Finite Element Analysis. John Wiley and Sons.

Argonne Code Center. Benchmark problem book. Technical report, ANL-7416, supplement 2, 1977.

Aussourd, C., 2003. A multidimensional AMR S_N scheme. Nucl. Sci. Eng. 143, 281–290.

Babuška, Rheinboldt, W.C., 1978. Error estimates for adaptive finite element computations. SIAM J. Numer. Anal. 15, 736–754.

Babuška, I., Strouboulis, T., 2001. The Finite Element Method and its Reliability. Clarendon Press, New York.

Bangerth, W., Joshi, A., 2008. Adaptive finite element methods for the solution of inverse problems in optical tomography. Inverse Problems 24 034011/1–22.

Bangerth, W., Rannacher, R., 2003. Adaptive Finite Element Methods for Differential Equations. Birkhäuser Verlag, Basel.

Bangerth, W., Hartmann, R., Kanschat, G., 2007. Deal.II – a general purpose object oriented finite element library. ACM Trans. Math. Software 33 (4), 24/1–24/27.

Bangerth, W., Hartmann, R., Kanschat, G., 2008. Deal.II differential equations analysis library, technical reference. http://www.dealii.org/.

Bangerth, W., 2008. A framework for the adaptive finite element solution of large inverse problems. SIAM J. Sc. Comput. 30, 2965–2989.

Bell, G., Glasstone, S., 1970. Nuclear Reactor Theory. Van Nostrand Reinhold Company, New York.

Braess, D., Verfürth, R., 1996. A posteriori error estimators for the Raviart-Thomas element. SIAM J. Numer. Anal. 33, 2431–2444.

Braess, D., 1997. Finite Elements. Cambridge University Press.

Brenner, S.C., Scott, R.L., 2002. The Mathematical Theory of Finite Elements, second ed. Springer, Berlin-Heidelberg-New York.

Carey, G.F., Oden, J.T., 1984. Finite Elements: Computational Aspects. Prentice-Hall.

Covington, LJ.,1995. Simulate-3: Advanced three-dimensional two-group reactor analysis code user's manual. Technical report, Studsvik/SOA-95/15, 1995.

Demkowicz, L., 2006. Computing with hp-Adaptive Finite Elements. Volume 1: One and Two Dimensional Elliptic and Maxwell Problems. Chapman & Hall.

Duderstadt, J., Hamilton, L., 1976. Nuclear Reactor Analysis. J. Wiley & Sons.

Duderstadt, J., Martin, W., 1979. Transport Theory. Wiley, New York.

Ferguson, D.R., Derstine, K.L., 1977. Optimized iteration strategies and data management considerations for fast reactor finite difference diffusion theory codes. Nucl. Sci. Eng. 64, 593–604.

Gago, J.P.de S.R., Kelly, D.W., Zienkiewicz, O.C., Babuška, I., 1983. A posteriori error analysis and adaptive processes in the finite element method: part II — Adaptive mesh refinement. Int. J. Num. Meth. Eng. 19, 1621–1656.

Jatuff, F.E., Gho, C.J., 1998. A physical interpretation and benchmarking of nodal diffusion error estimators. Ann. Nucl. Energy 25, 1235–1246.

Jatuff, F.E., 1995. Error estimators and adaptivity for the neutron diffusion problem. Ann. Nucl. Energy 22 (12), 775–786.

Jessee, J.P., Fiveland, W.A., Howell, L.H., Colella, P., Pember, R.B., 1998. An adaptive mesh refinement algorithm for the radiative transport equation. J. Comput. Phys. 139 (2), 380–398.

Kanschat, G., 1996. Parallel and adaptive galerkin methods for radiative transfer problems. Dissertation, Universität Heidelberg, 1996.

Kirk, B., Carey, GF., A parallel, adaptive finite element scheme for modeling chemotactic biological systems. Comm. Numer. Meth. Eng., submitted for publication.

Kirk, B., Peterson, J.W., Stogner, R.H., Carey, G.F., 2006. LibMesh: a C++ library for parallel adaptive mesh refinement/coarsening simulations. Eng. Comput. 22 (3–4), 237–254.

Klar, A., Lang, J., Seaïd, M., 2005. Adaptive solutions of SP_N-approximations to radiative heat transfer in glass. Int. J. Therm. Sci. 44, 1013–1023.

Krein, M.G., Rutman, M.A., 1962. Linear operators leaving invariant a cone in a Banach space. Amer. Math. Soc, 199–325. Translation.

Lautard, J.-J., Loubière, S., Fedon-Magnaud, C., 1990. Cronos: a modular computational system for neutronic core calculations. In: IAEA Specialists Meeting on Advanced Calculational Methods for Power Reactors. IAEA, Cadarache, France.

Lefebvre, LC., Mondot, J., West, JP., Benchmark calculations of power distribution within assemblies (specifications). Technical report, OECD/NEACRP-L-336, 1996.

Leicht, T., Hartmann, R., 2007. Anisotropic mesh refinement for discontinuous galerkin methods in two-dimensional aerodynamic flow simulations. Int. J. Numer. Meth. Fluid. 56 (11), 2111–2138.

Ragusa, J., 2004. 3-D adaptative solution of the multigroup diffusion equation on irregular structured grids using a non conforming finite element method formulation. In: Proceeding of the Physor 2004 International Conference: The Physics of Fuel Cycles and Advanced Nuclear Systems: Global Developments, Chicago, Illinois, 2004.

Ragusa, J., 2008. A simple Hessian-based 3D mesh adaptation technique with applications to the multigroup diffusion equations. Ann. Nucl. Energy 35, 2006–2018.

Richling, S., Meinköhn, E., Kryzhevoi, N., Kanschat, G., 2001. Radiative transfer with finite elements. Astron. Astrophys 380, 776–788.

The deal.II manual, documentation of the DerivativeApproximation class. http://www.dealii.org/ developer/doxygen/deal.II/ classDerivativeApproximation.html.

Wachspress, E.L., 1966. Iterative Solution of Elliptic Systems and Application to the Neutron Diffusion Equations of Reactor Physics. Prentice-Hall, Englewood Cliffs, NJ.

Wang, Y., Ragusa, J., 2006. Adaptive automated solution of the multigroup diffusion equations. In: International Conference on Physics of Reactors (PHYSOR 2006): Advances in Nuclear Analysis and Simulation, Vancouver, Canada, 2006.

Wang, Y., Ragusa, J., Application of hp-adaptivity to the multigroup diffusion equations. Nucl. Sci. Eng., in press.

Zhang, H., Lewis, E.E., 2001. An adaptive approach to variational nodal diffusion problems. Nucl. Sci. Eng. 137, 14–22.

Zhang, H., Lewis, E.E., 2002. Spatial adaptivity applied to the variational nodal P_N equations. Nucl. Sci. Eng. 142, 1–7.

Please cite this article in press as: Wang, Y., et al., Three-dimensional *h*-adaptivity for the multigroup neutron diffusion equations, Prog. Nucl. Energy (2009), doi:10.1016/j.pnucene.2008.11.005